ISSN 0015-4628, Fluid Dynamics, 2020, Vol. 55, no. 3, pp. 314–322. © Pleiades Publishing, Ltd., 2020.
Russian Text © The Author(s), 2020, published in Izvestiya RAN. Mekhanika Zhidkosti i Gaza, 2020, Vol. 55, No. 3, pp. 26–35.

A Study of Transient Flows with Interfaces Using Numerical Solution of Navier–Stokes Equations

A. I. Aleksyuk[a,b,*] and V. Ya. Shkadov[a,]**

[a] *Moscow State University, Moscow, Russia*

[b] *Water Problems Institute of RAS, Moscow, Russia*

**e-mail: aleksyuk@mech.math.msu.su*

***e-mail: shkadov@mech.math.msu.su*

Received November 7, 2019; revised December 17, 2019; accepted December 17, 2019

Abstract—Flows of two immisible fluids are considered taking into account the capillary and gravity forces. The flow is described using a viscous incompressible fluid model within a two-dimensional formulation. The Navier–Stokes equations are solved numerically by an extended finite-element method, which allows for the presence of a strong discontinuity on the interface. The interface location is tracked using the level set method. This approach makes it possible to study flows with a varying topology of the interface. The calculation results are presented for the problems of a rising 2D bubble, development of the Rayleigh–Taylor instability, and a film flowing down a vertical wall in an extended region.

Keywords: two-phase flows, Navier–Stokes equations, level set method, film flow, two-dimensional bubble, Rayleigh–Taylor instability

DOI: 10.1134/S0015462820030015

The mesh methods of modeling transient flows with interfaces can be separated into methods with explicit capturing of the interface on deformed meshes and the methods in which the location of the interface is determined using immovable meshes. In the first class of methods, during the calculation the interface coincides with a mesh line, which makes it possible to take into account fairly simply the discontinuities of the functions and their derivatives in the calculation scheme. The most widely encountered representatives of the second class are the volume of fluid method and the level set method. The advantage of the latter one is the fact that the interface is not smoothed and can be found implicitly using an auxiliary function, i.e. the level function, for which a transport equation is solved. This makes it possible to consider explicitly discontinuities of functions in the mathematical formulation of the method. The presence of discontinuities inside the cells can be taken into account, in particular, using an extended finite element method (XFEM) [1], in which the standard spaces of sampling and weighting functions is complemented by a set of functions which allow for discontinuities on the cells. The main advantage of the second class of methods is their higher universality, for instance, in modeling flows with a varying topology of the interface.

In the present paper, we describe a realization of the level set method in combination with the extended finite-element method [2–5] for modeling two-phase flows of immisible fluids in extended regions with the capillary forces, the gravity force, and possible complex deformations of the interface taken into account. The algorithms are tested with the reference to the examples of problems of a rising two-dimensional bubble and Rayleigh-Taylor instability. The results of applying this method to the problem of the development of a film flow in an extended region are also discussed.

1. FORMULATION OF THE PROBLEM

A two-dimensional flow of two incompressible viscous fluids separated by an interface $\Gamma_S(t)$ is described by the Navier–Stokes equations:

$$\mathbf{u}^\alpha_{,t} + (\mathbf{u}^\alpha \cdot \nabla)\mathbf{u}^\alpha = -\frac{1}{\rho^\alpha}\nabla \cdot \mathbf{P}^\alpha + \mathbf{F}, \tag{1.1}$$

$$\nabla \cdot \mathbf{u}^\alpha = 0. \tag{1.2}$$

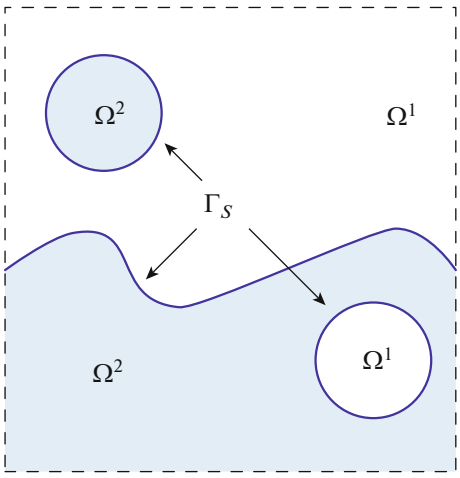

Fig. 1. Scheme of the two-phase flow region with an interface.

Here, subscript α takes values 1 and 2 for the parameters of the first and second fluid, respectively; ρ^α is the density; $\mathbf{u}^\alpha(\mathbf{x},t) = (u_1^\alpha, u_2^\alpha)$ and $\mathbf{F} = (F\cos\theta, F\sin\theta)$ are the vectors of velocity and mass forces; $\mathbf{P}^\alpha(\mathbf{x},t)$ is the stress tensor whose components take the following form in Cartesian coordinates $\mathbf{x} = (x_1, x_2)$:

$$P_{ij}^\alpha(\mathbf{x},t) = -p^\alpha\delta_{ij} + \mu^\alpha(u_{i,j}^\alpha + u_{j,i}^\alpha).$$

Here, $p^\alpha(\mathbf{x},t)$ and μ^α are the pressure and dynamic viscosity coefficient; δ_{ij} is the Kronecker delta; $(\cdot)_{,i} = \partial/\partial x_i$, and $(\cdot)_{,t} = \partial/\partial t$.

On the interface, the conditions are satisfied:

$$\mathbf{u}^1 = \mathbf{u}^2, \quad (\mathbf{P}^1 - \mathbf{P}^2)\cdot\mathbf{n} = \sigma\kappa\mathbf{n}, \quad \mathbf{x}\in\Gamma_S.$$

Here, σ and $\kappa(\mathbf{x},t)|_{\mathbf{x}\in\Gamma_S}$ are the constant surface tension coefficient and the curvature of the interface between the two fluids, and $\mathbf{n}$ is the normal vector. On the immovable boundaries of the flow domain considered Ω, the Dirichlet or Neumann conditions for the velocity are set or the stress vector are specified. At the initial instant, the position of the interface and the velocity field are known. We represent Ω as a combination of domains Ω^1 and Ω^2 (Fig. 1) occupied by the first and the second fluid and introduce the common notation for the parameters of both media, omitting superscript α; for instance, for pressure: $p(\mathbf{x},t) = p^\alpha(\mathbf{x},t)$, when $\mathbf{x}\in\Omega^\alpha$.

Let L_0, U_0, ρ_0, and μ_0 be the characteristic length, velocity, density, and viscosity (as the two latter parameters, the density and viscosity of one of the fluids can be chosen). After nondimensionalization using the formulas (the prime denotes dimensionless variables)

$$t' = \frac{tU_0}{L_0}, \quad \mathbf{x}' = \frac{\mathbf{x}}{L_0}, \quad \mathbf{u}' = \frac{\mathbf{u}}{U_0}, \quad p' = \frac{p}{\rho_0 U_0^2}, \quad \rho' = \frac{\rho}{\rho_0}, \quad \mu' = \frac{\mu}{\mu_0}, \quad \kappa' = \kappa L_0,$$

the following dimensionless parameters characterizing the flow appear in the problem formulation:

$$\mathrm{Re} = \frac{\rho_0 U_0 L_0}{\mu_0}, \quad \mathrm{We} = \frac{\sigma}{\rho_0 U_0^2 L_0}, \quad \mathrm{Fr} = \frac{U_0^2}{FL_0}, \quad \frac{\rho^1}{\rho^2}, \quad \frac{\mu^1}{\mu^2}.$$

In what follows, the primes in the dimensionless parameters are omitted.

2. NUMERICAL METHOD

In this section we describe the key issues of the method used. The main ideas of the algorithms realized in modeling the flows with interfaces and other variations of the methods used are discussed in detail

in [2–5]. To track the motion of the interface, the level set method [6] is used. The function $\varphi(\mathbf{x}, t)$ is introduced which has the following properties:

1. $\Gamma_S(t) = \{\mathbf{x} : \varphi(\mathbf{x}, t) = 0\}$;

2. $\varphi(\mathbf{x}, t) > 0$ if $\mathbf{x} \in \Omega^1$ and $\varphi(\mathbf{x}, t) < 0$ if $\mathbf{x} \in \Omega^2$;

3. $|\varphi(\mathbf{x}, t)| = \min_{\mathbf{x}_S \in \Gamma_S} |\mathbf{x} - \mathbf{x}_S|$.

The first two properties of this function are retained if it satisfies the transport equation

$$\varphi_{,t} + \mathbf{u} \cdot \nabla\varphi = 0. \tag{2.1}$$

The third condition makes it possible to find the normal direction to the interface using the formula $\mathbf{n} = \nabla\varphi$ for $\mathbf{x} \in \Gamma_S$. However, to keep this property satisfied, it is necessary to perform periodically a re-initialization of the function $\varphi(\mathbf{x}, t)$ to ensure that this condition is satisfied and keep unchanged the position of the interface ($\varphi(\mathbf{x}, t) = 0$).

The initial-boundary-value problem for the Navier–Stokes equations is solved numerically using a GLS (Galerkin/Least-Squares) stabilized finite-element method. Possible discontinuities of the solution and its derivatives on the interface are described using the extended finite-element method (XFEM) [1–5]. The calculation domain Ω is represented as a combination of the rectangles Ω_e, $e = 1, \ldots, n_e$, of a regular mesh with steps Δ_1, Δ_2 along the x_1 and x_2 coordinates, with the mesh having m nodes $\mathbf{x}_i$. The standard finite-dimension approximations of the spaces of sampling and weighting functions on the mesh are complemented with the functions which allow for strong pressure discontinuities in the cells containing the interface. An approximate solution $\mathbf{u}^h$, p^h is sought in the form

$$\mathbf{u}^h(\mathbf{x}, t) = \sum_{i=1}^{m} \mathbf{v}_i N_i(\mathbf{x}); \quad p^h(\mathbf{x}, t) = \sum_{i=1}^{m} p_i N_i(\mathbf{x}) + \sum_{k=1}^{m^*} p_k^* M_k(\mathbf{x}, t). \tag{2.2}$$

Here, $\mathbf{v}_i$, p_i, p_k^* are the coefficients to be found which depend on time; $N_i(\mathbf{x})$ are piecewise bilinear continuous functions, and $N_i(\mathbf{x}_j) = \delta_{ij}$; $i = 1, \ldots, m$, $j = 1, \ldots, m$, $k = 1, \ldots, m^*$. The second summation in the expression for p^h is performed over the nodes of each cell containing the interface. On these cells, the functions $M_k(\mathbf{x}, t)$ are determined as follows:

$$M_k(\mathbf{x}, t) = N_k^*(\mathbf{x})\big[\psi(\mathbf{x}, t) - \psi(\mathbf{x}_k, t)\big], \quad \psi(\mathbf{x}, t) = \begin{cases} -1, & \varphi(\mathbf{x}, t) < 0 \\ 0, & \varphi(\mathbf{x}, t) = 0 \\ 1, & \varphi(\mathbf{x}, t) > 0. \end{cases}$$

Here, N_k^* is the constriction of function N_k onto the cells containing interface Γ_S. We note that for the velocity in (2.2) we use a standard approximation. Time discretization was performed using an Euler implicit scheme of the first order with a constant step Δt. To avoid the explicit calculation of curvature κ in the numerical solution, we used the approach described, for instance, in [2] which is based on the application of the Laplace–Beltrami operator.

The transport equation (2.1) is also solved by a stabilized finite-element method. In each global time iteration, we used the method of successive approximations, which made it possible to adjust the solutions of motion equations (1.1)–(1.2) and of Eq. (2.1) for determining the interface. A system of linear algebraic equations with an ill-posed matrix for Eqs. (1.1)–(1.2) is solved by a direct LU-decomposition method which makes it possible to avoid the problem associated with poor convergence of iteration methods due to the expansion of the spaces of sampling and weighting functions [8].

The stabilized finite-element method used in this study was successfully applied by the authors of [9–11] to studying 2D and 3D single-fluid flows past bodies. In addition, in those papers one can find the results of testing the method for single-phase flows and the details of algorithms. In the next sections of the paper, we will present the results of applying the method described above to solving three problems with interfaces. The first two problems are the classical examples of testing numerical algorithms for two-phase flows (for instance, see [12, 13]). The third problem is the demonstration of capacity of the method to calculate flows in extended regions with restructuring wave patterns.

Table 1. Regimes of rise of the "2D bubble" considered in the study

Regime	ρ^1 (kg/m^3)	ρ^2 (kg/m^3)	μ^1 (kg/(m · s))	μ^2 (kg/(m · s))	σ (kg/s^2)	$\Delta_1(=\Delta_2), \Delta t$
I	1000	100	10	1	24.5	0.02, 0.002
II	1000	1	10	0.1	1.96	0.005, 0.001

3. RESULTS OF THE APPLICATION OF THE METHOD

3.1. A rising "Two-Dimensional Bubble"

Two regimes of rise of a 2D bubble are modeled taking into account capillary forces (see Table 1). These regimes are artificial tests [12]. In the first of them the parameters are chosen so that the bubble is deformed only slightly (Fig. 2a). In the second example, at a certain instant of time the topology of the interface changes: from the main bubble secondary bubbles separate (Fig. 2b). In [12], the numerical results obtained using computer codes of three independent groups of researches are presented. Below, the results are represented in dimensional form for convenience of comparison with [12]. At the initial instant of time, both fluids are at rest and the interface is a circle with the radius of 0.25 m and the center located at the point $x_1 = 0.5$ m, $x_2 = 0.5$ m. In the gravity field $F = 0.98$ m/s^2, $\theta = -\pi/2$ the light-weight fluid (2D bubble) starts rising. The flow domain is a rectangle $\{0 \le x_1 \le 1; 0 \le x_2 \le 2\}$, on whose boundaries $x_2 = 0$, $x_2 = 2$ the no-slip condition is satisfied, and on the boundaries $x_1 = 0$, $x_1 = 1$ the slip conditions are specified. The comparison of the interface shape at $t = 3$ s and the time dependence of the ordinate of the bubble center of mass with the data from [12] is given in Fig. 3. A noticeable quantitative difference is observed only in describing the process of separation of secondary bubbles, with the other results being in good agreement. The authors of [12] note that in the second test all three computer codes considered also give different results for the process of separation of secondary bubbles, despite the fact that the results completely coincide until the beginning of this process (the same is true for the first test as well). In Fig. 3, it is clear that the present calculations lie most close to those obtained by the MooNMD algorithm in which deformed meshes were used, with the nodes traveling together with the interface.

3.2. Rayleigh–Taylor Instability

Two liquid layers separated by a horizontal interface are at rest in the gravity field. The situation is considered when this equilibrium is unstable. The density of the upper liquid is greater than that of the lower liquid. At the initial instant of time, small disturbances of the interface are introduced. The capillary forces are neglected.

Figure 4 shows the comparison with the data [13] for the parameters described below. The flow domain is a rectangle $\{0 \le x_1 \le 1; 0 \le x_2 \le 2\}$ with the no-slip conditions on the boundary. The disturbance at the interface at the initial instant of time is specified by the equation $x_2 = 1 - 0.15\sin 2\pi x_1$. The densities of the fluids differ in 1.8 times and the kinematic viscosities of the fluids coincide. The Reynolds number is $R = 420$ (the characteristic linear scale L_0 is the length of the domain along the x_1-coordinate and the characteristic velocity $U_0 = \sqrt{L_0 g}$, where g is the gravity force acceleration).

The calculations were performed on the grid with the spatial and time steps $\Delta_1 = \Delta_2 = 0.01$, $\Delta t = 0.005$. For comparison, in Fig. 4 we present the data obtained in [13] using the level set method on the 312 × 614 grid. Despite a qualitative agreement, the results have some differences which may be associated with the mesh resolution.

3.3. A Film Falling Down a Vertical Wall

We will consider five regimes of a film flow down a vertical plane, which are presented in Table 2. As the characteristic dimensional parameter scales, we chose density ρ_0, dynamic viscosity μ_0, film thickness L_0, and characteristic velocity $U_0 = gL_0^2\rho_0/(3\mu_0)$. The parameters of the second fluid are chosen so that their influence on the flow is insignificant: $\rho^1/\rho^2 = 10^3$, $\mu^1/\mu^2 = 5\times10^{-3}$.

At the initial instant, interface Γ_S is described by the formula $x_2 = 1$ and the flow parameters correspond to a steady-state solution with the parabolic velocity profile $u_1(\mathbf{x}, 0) = 1.5x_2(2 - x_2)$, $u_2(\mathbf{x}, 0) = 0$. On the plane vertical wall ($x_2 = 0$), the no-slip condition is specified. On the inlet boundary ($x_1 = 0$), the

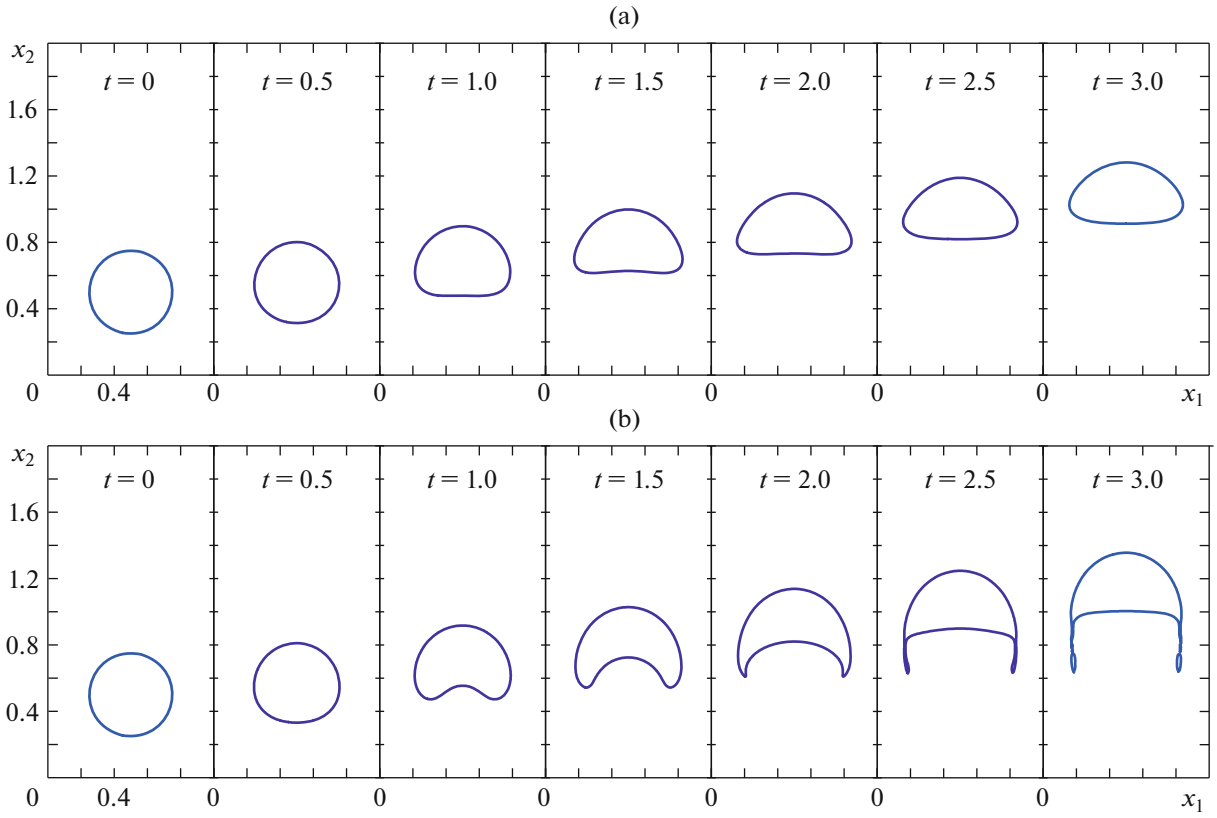

Fig. 2. Evolution of the boundary of a rising "two-dimensional bubble" for regimes I (a) and II (b).

film thickness is fixed and the periodic velocity fluctuation is specified: $u_1(0, x_2, t) = 1.5x_2(2 - x_2)[1 + a\sin(2\pi ft)]$, $u_2(0, x_2, t) = 0$, where a and f are the given amplitude and frequency of velocity fluctuations at the inlet. At the outlet ($x_1 = L$), we specify the soft boundary conditions $u_{1,1}(L, x_2, t) = u_{2,1}(L, x_2, t) = 0$. The dimensions of the calculation domain, the spatial and time steps, and the values of the parameters Re, We, and f are given in Table 2 (the amplitude $a = 0.03$ for regimes B–E and $a = 0.1$ for regime A).

The dependences of the film thickness on the longitudinal coordinate for regimes A–E are shown in Fig. 5. The initial stage of the wave development can be described using the linear stability theory. After linearization of the Shkadov evolutionary equations [14], using the normal mode method (the film thickness is sought in the form $h(x_1, t) = 1 + \varepsilon \exp i(kx_1 - \omega t)$), we obtain the dispersion equation

$$\frac{1}{3}\mathrm{ReWe}k^4 - \frac{2}{5}\mathrm{Re}k^2 + \left(3i + \frac{4}{5}\omega\mathrm{Re}\right)k - \frac{1}{3}\mathrm{Re}\omega^2 - i\omega = 0. \qquad (3.1)$$

Table 2. Regimes of the falling film flow considered and the complex wave numbers found from the solutions of dispersion equations (3.1) and (3.2) with a positive phase velocity and minimal (in absolute value) negative amplification factor k_i for $\omega = f/2\pi$

Regime	Re	We	f	Region	$\Delta_1, \Delta_2, \Delta t$	k – solution (3.1)	k – solution (3.2)
A	16.2	46.87	0.0054	1500 × 5	1, 0.1, 0.0050	$0.01138 - 0.00068i$	$0.01141 - 0.00082i$
B	16.2	46.87	0.0252	600 × 2.2	1, 0.1, 0.0025	$0.05847 - 0.01147i$	$0.06028 - 0.01294i$
C	16.2	46.87	0.0404	1000 × 2.5	1, 0.1, 0.0020	$0.10260 - 0.01787i$	$0.10680 - 0.01882i$
D	16.2	46.87	0.0718	1500 × 5	1, 0.1, 0.0050	$0.17656 - 0.00861i$	$0.18236 - 0.00819i$
E	32.4	46.87	0.0718	1500 × 5	1, 0.1, 0.0050	$0.17839 - 0.00453i$	$0.18390 - 0.00426i$

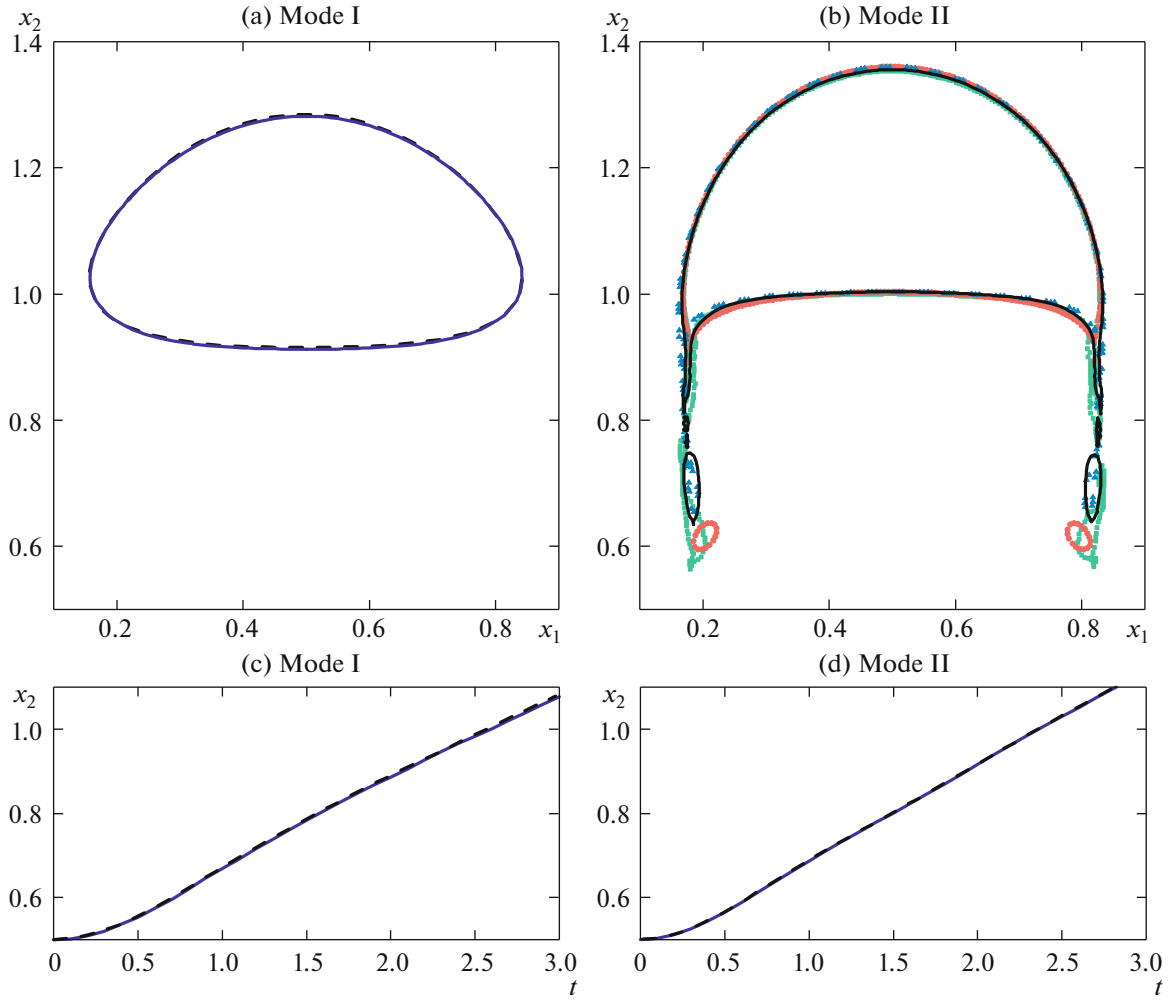

Fig. 3. The bubble surface at $t = 3$ (a, b) and the time evolution of the x_2-coordinate of the center of mass of the rising "2D bubble" (c, d) for regimes I (a, c) and II (b, d). The solid line shows the present calculations; the dashed line and dots show the results of [12]; three different markers of the dots in figure (b) correspond to the calculations using three different computer codes; in figures (a, c, d) the dashed line corresponds to the calculations using the MooNMD code [12] (for regime I, in the scale of the figures the results obtained using two other programs lie on the shown dashed curves).

We also consider the dispersion equation obtained from the second-order equations [15], in which a deviation of the parabolic velocity profile used in the Kapitsa–Shkadov method is taken into account:

$$\frac{1}{3}\mathrm{ReWe}k^4 + \frac{12}{5}ik^3 - \left(\frac{18}{35}\mathrm{Re} + \frac{9}{5}i\omega\right)k^2 + \left(3i + \frac{34}{35}\omega\mathrm{Re}\right)k - \frac{2}{5}\mathrm{Re}\omega^2 - i\omega = 0. \qquad (3.2)$$

In Eqs. (3.1) and (3.2), a complex wave number $k = k_r + ik_i$ is sought, and frequency ω is assumed to be known and related to the forced frequency at the inlet as $f = 2\pi\omega$. If the amplification factor k_i is negative (positive), the waves grow (attenuate) in the space. A detailed derivation of the dispersion equations is given, for instance, in [15].

For the case considered, Eqs. (3.1) and (3.2) have three roots corresponding to growing solutions, and one root corresponding to an attenuating solution. For example, for regime E the roots of the dispersion equation (3.1) are:

$$0.1784 - 0.0045i; \quad 0.1073 - 0.2346i; \quad -0.3558 - 0.0217i; \quad 0.0700 + 0.2609i. \qquad (3.3)$$

The solutions realized in the numerical modeling of regimes A–E correspond to the roots with a positive phase velocity and minimal (in absolute value) amplification factor $k_i < 0$, i.e., the first root in this case. The coorresponding roots for each regime are given in Table 2. In Figs. 5b–5e, we present the com-

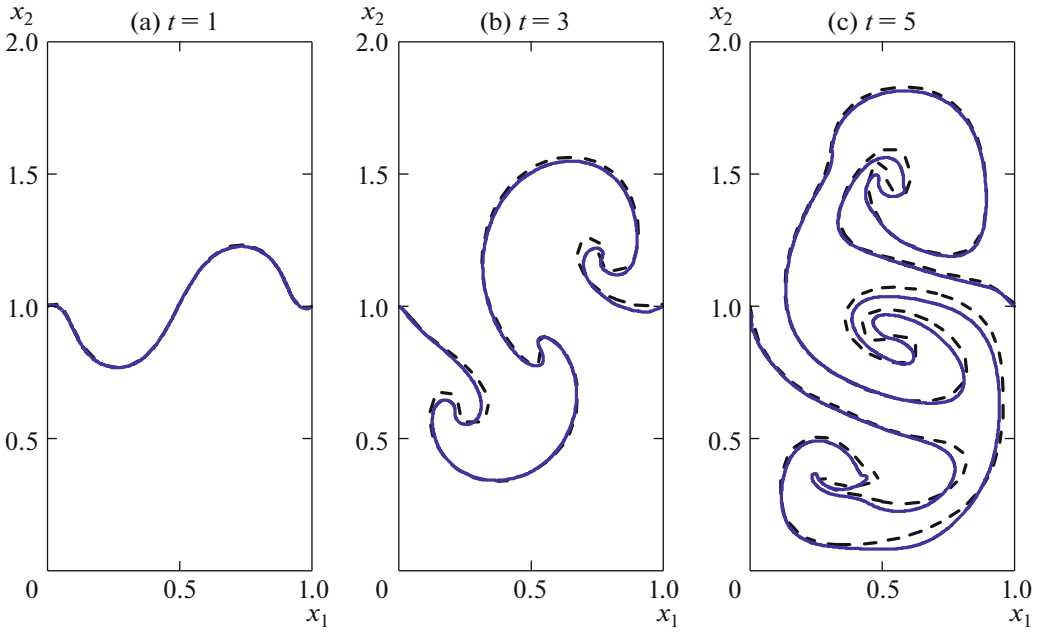

Fig. 4. Evolution of the interface between a heavy and a light-weight fluid in the Rayleigh–Taylor instability problem. The interface is shown for $t = 1$ (a), 3 (b), and 5 (c). The solid line shows the present results obtained on a 100 × 200 mesh; the dashed line shows the data [13] obtained on a 312 × 624 mesh.

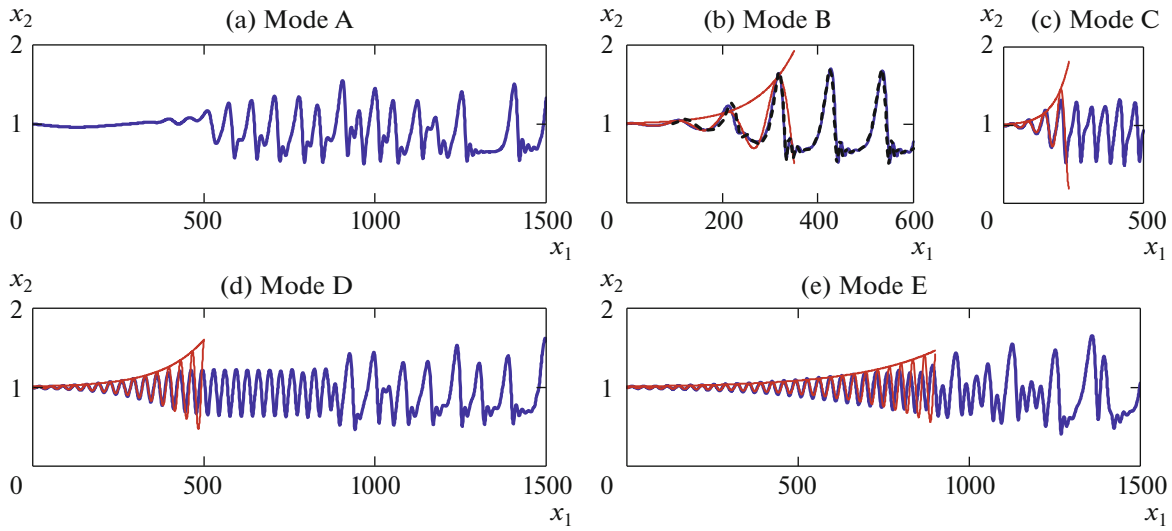

Fig. 5. The interface for regimes A–E: the solid line (blue) shows the present calculations; the dashed line (black) in figure (b) shows the data [16]; the thin solid line (red) shows the linear stage of disturbance development corresponding to the solution of Eq. (3.2).

parison of the calculation results with the linear theory based on dispersion equation (3.2). As is clear, for all regimes considered the amplification factors of the disturbances and the wave numbers agree well. The solution of the classical dispersion equation (3.1) gives similar values (see Table 2): the frequency differs by no more than 4%, the difference in the amplification factor is as large as 11% and 16% for low frequencies (regimes A and B). In Fig. 5a, we do not give a comparison with the linear theory because in this case, on the background of low-frequency waves determined by the inlet frequency, more unstable high-frequency disturbances start to grow fairly rapidly (see Fig. 5a at $x_1 \approx 400$).

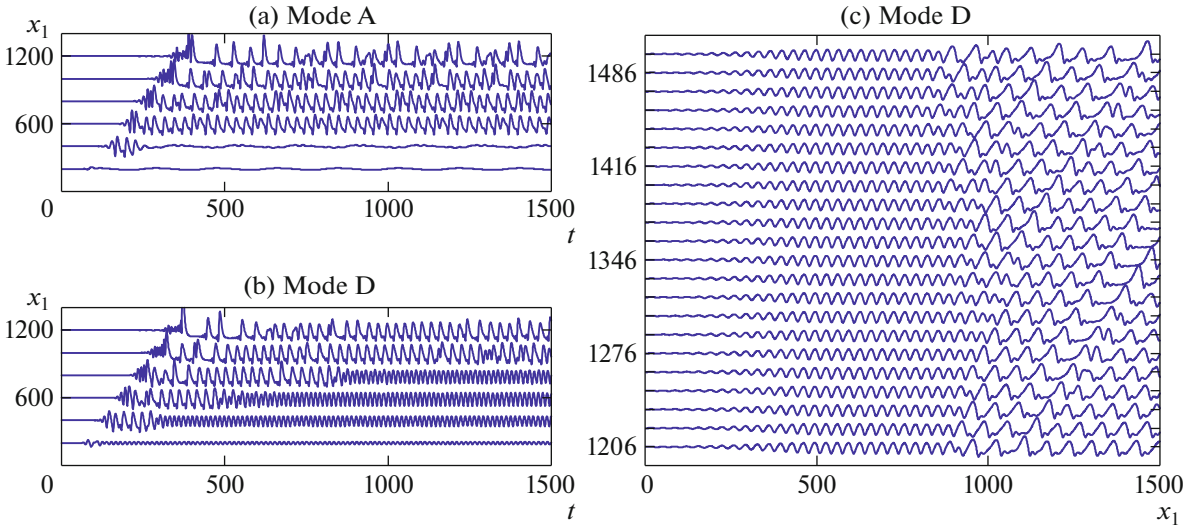

Fig. 6. Temporal and spatial evolution of the interface for regimes A and D: (a, b) show the time dependences of the film thickness for regimes A and D at the points $x_1 = 200$; 400; 600; 800; 1000; and 1200; (c) shows the interface for regime D at different instants of time with the step $\Delta t = 14$ (the value $1/\Delta t \approx 0.0714$ is close to the frequency at the inlet, $f = 0.0718$).

Regimes B–D were modeled earlier in [16] (see Figs. 2a, 2b, and 2d in [16]). In that study, a finite-difference marker-and-cell method was applied to single-phase flows on grids with $\Delta_1 = 0.436$, $\Delta_2 = 0.08333$, and $\Delta t = 0.01$. The calculation results agree with each other. This is clear, for instance, from the comparison of the nonlinear wave formation stage and the limiting wave regime in Fig. 5b. It should be noted that the limiting regimes are also well reproduced by finding the optimal waves of the global attractor [17], determined on the basis of integral evolutionary equations [14].

The development of wave structures can be tracked using the graphs of the time dependence of the film thickness at fixed points of space and the time variation of the interface shown in Fig. 6. An interesting specific feature arising in the numerical modeling is a wave propagating into the region of the wave-free solution. For regimes A and D (with the maximal difference in disturbance frequency in the inlet section), it is clear from Figs. 6a, 6b that this wave propagates with a similar velocity, approximately equal to 4. However, for regime A the front boundary in the plane (t, x_1) is slightly shifted to the right, which is associated with the difference of the disturbance frequency in the inlet section. In addition, during a certain time interval after the passage of the wave the time dependence of the film thickness is qualitatively repeated for regimes A and D. In Fig. 6c, two transitional stages are clearly manifested. First, as a result of the loss of stability of the wave-free regime regular waves are formed. These waves also turn out to be unstable, and the second region of transition to the limiting wave regime arises. The boundary of the regular wave regime can be displaced at the distances of the order of hundred film thicknesses.

SUMMARY

The results of the application of a level set method in combination with an extended finite-element method to numerical solution of the Navier–Stokes equations describing two-phase flows with an interface are presented. Three problems of flows with interfaces are considered: a rising 2D bubble, development of the Rayleigh–Taylor instability, and a film falling down a vertical wall. In all cases, the results agree with the data of other authors. The approach described makes it possible to perform quantitative calculations of transient two-phase flows with interfaces in extended domains and the flows with varying topology of the interface.

FUNDING

The work obtained financial support from the Russian Foundation for Basic Research (projects nos. 18-01-00762 and 18-51-00006).

REFRENCES

1. N. Moës, J. Dolbow, and T. Belytschko, "A finite element method for crack growth without remeshing," Int. J. Numer. Meth. Eng. 46 (1), 131–150 (1999). https://doi.org/10.1002/(SICI)1097-0207(19990910)46:1<131::AID-NME726>3.0.CO;2-J
2. T.P. Fries, "The intrinsic XFEM for two-fluid flows," Int. J. Numer. Methods Fluids 60, (4), 437–471 (2009). https://doi.org/10.1002/fld.1901
3. T.P. Fries and T. Belytschko, "The extended/generalized finite element method: An overview of the method and its applications," Int. J. Numer. Meth. Eng. 84 (3), 253–304 (2010). https://doi.org/10.1002/nme.2914
4. H. Sauerland, *An XFEM Based Sharp Interface Approach for Two-Phase and Free-Surface Flows* (Diss. RWTH Aachen, 2013).
5. H. Sauerland and T.P. Fries, "The extended finite element method for two-phase and free-surface flows: A systematic study," J. Comput. Phys. 230 (9), 3369–3390 (2011). https://doi.org/10.1016/j.jcp.2011.01.033
6. S. Osher and R.P. Fedkiw, "Level set methods: An overview and some recent results," J. Comput. Phys. 169 (2), 463–502 (2001). https://doi.org/10.1006/jcph.2000.6636
7. T.J.R. Hughes, L.P. Franca and G.M. Hulbert, "A new finite element formulation for computational fluid dynamics: VIII. The Galerkin/least-squares method for advective-diffusive equations," Comput. Methods in Appl. Mech. Eng. 73 (2), 173–189 (1989). https://doi.org/10.1016/0045-7825(89)90111-4
8. I. Babuška and U. Banerjee, "Stable generalized finite element method (SGFEM)," Comput. Methods in Appl. Mech. Eng. 201–204, 91–111 (2012). https://doi.org/10.1016/j.cma.2011.09.012
9. A.I. Aleksyuk and V.Y. Shkadov, "Analysis of three-dimensional transition mechanisms in the near wake behind a circular cylinder," Eur. J. Mech. B/Fluids 72, 456–466 (2018). https://doi.org/10.1016/j.euromechflu.2018.07.011
10. A.I. Aleksyuk and A.N. Osiptsov, "Direct numerical simulation of energy separation effect in the near wake behind a circular cylinder," Int. J. Heat Mass Transfer 119, 665–677 (2018). https://doi.org/10.1016/j.ijheatmasstransfer.2017.11.133
11. A.I. Aleksyuk, "Influence of vortex street structure on the efficiency of energy separation," Int. J. Heat Mass Transfer 135, 284–293 (2019). https://doi.org/10.1016/j.ijheatmasstransfer.2019.01.103
12. S. Hysing, S. Turek, D. Kuzmin, et al., "Quantitative benchmark computations of two-dimensional bubble dynamics," Int. J. Numer. Methods Fluids 60 (11), 1259–1288 (2009). https://doi.org/10.1002/fld.1934
13. N. Grenier, M. Antuono, A. Colagrossi, et al., "An Hamiltonian interface SPH formulation for multi-fluid and free surface flows," J. Comput. Phys. 228 (22), 8380–8393 (2009). https://doi.org/10.1016/j.jcp.2009.08.009
14. V.Y. Shkadov, "Wave flow regimes of a thin layer of viscous fluid subject to gravity," Fluid Dynamics 2 (1), 29–34 (1967).
15. S. Kalliadasis, C. Ruyer-Quil, B. Scheid, and M.G. Velarde, "*Falling liquid films*," *Applied mathematical sciences* (Springer London, London), 2012, vol. 176. https://doi.org/10.1007/978-1-84882-367-9
16. T. Nosoko and A. Miyara, "The evolution and subsequent dynamics of waves on a vertically falling liquid film," Phys. Fluids 16 (4), 1118–1126 (2004). https://doi.org/10.1063/1.1650840
17. A.N. Beloglazkin, V.Y. Shkadov, and A.E. Kulago, "Limiting wave regimes uring the spatial and temporal development of disturbances in falling liquid films," Moscow University Mechanics Bulletin 74 (3), 69–73 (2019).